J|A|C|S ARTICLES

Published on Web 03/10/2010

Transition from Tunneling to Hopping Transport in Long, Conjugated Oligo-imine Wires Connected to Metals

Seong Ho Choi,[†] Chad Risko,[‡] M. Carmen Ruiz Delgado,[‡] BongSoo Kim,[†] Jean-Luc Brédas,[‡] and C. Daniel Frisbie*,[†]

Department of Chemistry and Department of Chemical Engineering and Materials Science, University of Minnesota, Minneapolis, Minnesota 55455, and School of Chemistry and Biochemistry and Center for Organic Photonics and Electronics (COPE), Georgia Institute of Technology, Atlanta, Georgia 30332

Received December 14, 2009; E-mail: frisbie@cems.umn.edu

Abstract: We report the electrical transport characteristics of conjugated oligonaphthalenefluoreneimine (ONI) wires having systematically varied lengths up to 10 nm. Using aryl imine addition chemistry, ONI wires were built from gold substrates by extending the conjugation length through imine linkages between highly conjugated building blocks of alternating naphthalenes and fluorenes. The resistance and current−voltage characteristics of ONI wires were measured as a function of molecular length, temperature, and electric field using conducting probe atomic force microscopy (CP-AFM). We have observed a transition in direct current (DC) transport from tunneling to hopping near 4 nm as previously established for oligophenyleneimine (OPI) wires. Furthermore, we have found that long ONI wires are less resistive than OPI wires. The single-wire conductivity of ONI wires is $\sim 1.8 \pm 0.1 \times 10^{-4}$ S/cm, a factor of ~2 greater than that of OPI wires, and consistent with the lower transport activation energy (~0.58 eV versus 0.65 eV or 13 versus 15 kcal/mol). Quantum chemical calculations reveal that charge is preferentially localized on the fluorene subunits and that the molecules are substantially twisted. Overall, this work confirms that imine addition chemistry can be used to build molecular wires long enough to probe the hopping transport regime. The versatility of this chemistry, in combination with CP-AFM, opens up substantial opportunities to probe the physical organic chemistry of hopping conduction in long conjugated molecules.

Introduction

Understanding electrical conduction in molecules is a long-standing goal in chemistry that is motivated by the importance of inter- and intramolecular electron transfer in biological processes (e.g., photosynthesis and enzyme catalysis)[1,2] and also by emerging applications of conjugated molecular films in electronic devices[3] such as transistors,[4−6] diodes,[7−9] and sensors.[10,11] The most direct way to probe conduction in molecules is to connect them between electrodes so that their current−voltage ($I-V$) characteristics can be recorded directly, a strategy that is clearly challenging because of the nanoscopic dimensions of molecules and the need for reliable chemistry to orient and fix the molecules in place. Nevertheless, several reliable techniques for making metal, semiconductor, or conducting polymer contacts to molecules have been developed over the past decade.[12−20] The development of these methods has created unprecedented opportunities for detailed, systematic examination of structure-transport relationships in molecules, e.g., the role of bond architecture,[16,21,22] molecular length,[22−25] and contact chemistry[26−32] in molecular conduction.

[†] University of Minnesota.
[‡] Georgia Institute of Technology.

(1) Nelson, D. L.; Cox, M. M. *Lehninger Principles of Biochemistry*; W. H. Freeman: New York, 2005.
(2) Schwarz, G.; Mendel, R. R.; Ribbe, M. W. *Nature* **2009**, *460*, 839–847.
(3) Mantooth, B. A.; Weiss, P. S. *Proc. IEEE* **2003**, *91*, 1785–1802.
(4) Kubatkin, S.; Danilov, A.; Hjort, M.; Cornil, J.; Bredas, J.-L.; Stuhr-Hansen, N.; Hedegard, P.; Bjornholm, T.*Nature* **2003**, *425*, 698–701.
(5) Moth-Poulsen, K.; Bjornholm, T. *Nat. Nanotechnol.* **2009**, *4*, 551–556.
(6) Park, J.; Pasupathy, A. N.; Goldsmith, J. I.; Chang, C.; Yaish, Y.; Petta, J. R.; Rinkoski, M.; Sethna, J. P.; Abruna, H. D.; McEuen, P. L.; Ralph, D. C. *Nature* **2002**, *417*, 722–725.
(7) Metzger, R. M. *Chem. Rev.* **2003**, *103*, 3803–3834.
(8) Heath, J. R.; Ratner, M. A. *Phys. Today* **2003**, *May*, 43–49.
(9) Chen, J.; Reed, M. A.; Rawlett, A. M.; Tour, J. M. *Science* **1999**, *286*, 1550–1552.
(10) Blum, A. S.; Kushmerick, J. G.; Long, D. P.; Patterson, C. H.; Yang, J. C.; Henderson, J. C.; Tour, J. M.; Shashidhar, R.; Ratna, B. R. *Nat. Mater.* **2005**, *4*, 167–172.
(11) McQuade, D. T.; Pullen, A. E.; Swager, T. M. *Chem. Rev.* **2000**, *100*, 2537–2574.
(12) Selzer, Y.; Allara, D. L. *Annu. Rev. Phys. Chem.* **2006**, *57*, 593–623.
(13) Wang, W.; Lee, T.; Reed, M. A. *Phys. Rev. B* **2003**, *68*, 035416.
(14) Salomon, A.; Cahen, D.; Lindsay, S.; Tomfohr, J.; Engelkes, V. B.; Frisbie, C. D. *Adv. Mater.* **2003**, *15*, 1881–1890.
(15) McCreery, R. L. *Chem. Mater.* **2004**, *16*, 4477–4496.
(16) McCreery, R. L.; Bergren, A. J. *Adv. Mater.* **2009**, *21*, 1–20.
(17) Kronemeijer, A. J.; Akkerman, H. B.; Kudernac, T.; Wees, B. J. v.; Feringa, B. L.; Blom, P. W. M.; deBoer, B. *Adv. Mater.* **2008**, *20*, 1467–1473.
(18) Akkerman, H. B.; Naber, R. C. G.; Jongbloed, B.; vanHalt, P. A.; Blom, P. W. M.; deLeeuw, D. M.; deBoer, B. *Proc. Natl. Acad. Sci. U.S.A.* **2007**, *104*, 11161–11166.
(19) Cai, L.; Cabassi, M. A.; Yoon, H.; Cabarcos, O. M.; McGuiness, C. L.; Flatt, A. K.; Allara, D. L.; Tour, J. M.; Mayer, T. S. *Nano Lett.* **2005**, *5*, 2635–2372.
(20) Akkerman, H. B.; Blom, P. W. M.; deLeeuw, D. M.; deBoer, B. *Nature* **2006**, *441*, 69–72.

 10.1021/ja910547c

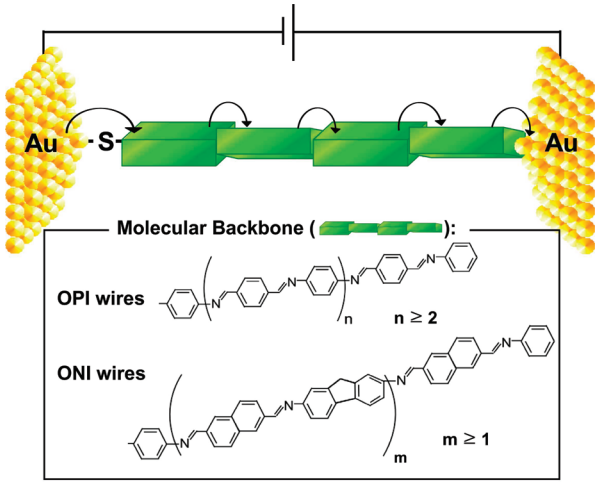

Figure 1. Schematic representation of hopping transport in a metal−molecule−metal junction (top) and structures of OPI and ONI wires (bottom). Green rectangular boxes represent conjugated subunits (local hopping sites) for charge carriers (electrons or holes). Curved arrows represent charge hopping over thermal barriers between local sites. In long wires, where tunneling is suppressed, hopping transport can be the principal transport mechanism (OPI, $n \geq 2$ and ONI, $m \geq 1$). The charge conduction process can be viewed as a series of discrete steps involving first injection of charge into the molecular orbitals, field-induced hopping of the charge carrier down the length of the molecule, and finally extraction of the charge into the receiving contact.

To date, the majority of measurements on molecular junctions have been made in the direct tunneling regime. That is, the molecules spanning the interelectrode gap are short enough that electrons tunnel directly from one contact to the other. The efficiency (length dependence) of this tunneling process depends on the architecture of the molecular backbone, and there are many intriguing effects that remain to be resolved concerning the role of the contacts, the electronic structures of the molecules, and the influence of intermolecular interactions. However, it is also interesting to consider the role of molecular structure in the hopping regime, that is, in situations where molecules are long enough that direct electrode-to-electrode tunneling is not possible and instead charge must be injected onto the molecular backbone and driven along the molecule by the applied electric field (see Figure 1). Hopping conduction is a principal charge conduction mechanism in thin films of conjugated organic molecules employed in devices.[33] Consequently, a richer understanding of the microscopic hopping conduction process along individual conjugated "molecular wires" may ultimately aid efforts to make better polymer semiconductors for applications in organic solar cells,[34,35] thin film transistors,[36,37] and light emitting diodes.[38,39] Transport in the hopping regime at nanoscopic length scales is almost entirely unexplored because of the difficulties associated with contacting sufficiently long conjugated molecules.

Recently, we[23] and others[40,41] have shown that it is possible to build long conjugated molecular wires attached to metal electrodes and to probe direct current (DC) transport as a function of length. In our work, we employed aryl imine addition chemistry to build oligophenyleneimine (OPI) wires up to 7 nm in length. In principle, an attractive feature of the aryl imine chemistry is that it is adaptable to other types of molecular building blocks, affording opportunities to examine wire conduction as a function of precisely controlled chain architecture.

Here we have taken the next steps in this direction by demonstrating that the imine addition chemistry can be employed to assemble wires from larger conjugated molecular building blocks based on naphthalene dialdehydes and fluorene diamines. The resulting oligonaphthalenefluoreneimine (ONI) wires are longer than the OPI wires (the structure is shown in Figure 1); we have achieved wires up to 10 nm in length, though our data suggest that longer wires could be grown. Using conducting probe atomic force microscopy (CP-AFM) to measure the $I-V$ characteristics of the wires, we observed a clear change in the transport mechanism from tunneling to hopping as a function of ONI wire length, consistent with prior studies of electron transfer in solution,[42−45] and our previous report on OPI wires.[23] The change in mechanism is manifested by self-consistent changes in the length, temperature, and electric field dependence of the $I-V$ characteristics. To our knowledge the ONI wires described here are the longest wires to date to be examined systematically in terms of length, temperature, and field dependence of conduction. In addition, we show that in some respects the ONI wires are a better system for transport studies than the original OPI wires. Specifically, the ONI wires grow perpendicular to the gold substrate, which lessens the uncertainties regarding intermolecular hopping in the conduction path. We also describe detailed quantum chemical calculations of the structure and charge distributions in the ONI wires in an effort to understand the key geometrical aspects of the wire

(21) Venkataraman, L.; Klare, J. E.; Nuckolls, C.; Hybertsen, M. S.; Steigerwald, M. L. *Nature* **2006**, *442*, 904–907.
(22) Liu, H.; Wang, N.; Zhao, J.; Guo, Y.; Yin, X.; Boey, F. Y. C.; Zhang, H. *ChemPhysChem* **2008**, *9*, 1416–1424.
(23) Choi, S. H.; Kim, B.-S.; Frisbie, C. D. *Science* **2008**, *320*, 1482–1486.
(24) Kim, B.-S.; Beebe, J. M.; Jun, Y.; Zhu, X. Y.; Frisbie, C. D. *J. Am. Chem. Soc.* **2006**, *128*, 4970–4971.
(25) Engelkes, V. B.; Beebe, J. M.; Frisbie, C. D. *J. Am. Chem. Soc.* **2004**, *126*, 14287–14296.
(26) Venkataraman, L.; Klare, J. E.; Tam, I. W.; Nuckolls, C.; Hybertsen, M. S.; Steigerwald, M. L. *Nano Lett.* **2006**, *6*, 458–462.
(27) Venkataraman, L.; Park, Y. S.; Whalley, A. C.; Nuckolls, C.; Hybertsen, M. S.; Steigerwald, M. L. *Nano Lett.* **2007**, *7*, 502–506.
(28) Xu, B.; Tao, N. J. *Science* **2003**, *301*, 1221–1223.
(29) Chen, F.; Li, X.; Hihath, J.; Huang, Z.; Tao, N. *J. Am. Chem. Soc.* **2006**, *128*, 15874–15881.
(30) Haick, H.; Cahen, D. *Prog. Surf. Sci.* **2008**, *83*, 217–261.
(31) Thieblemont, F.; Seitz, O.; Vilan, A.; Cohen, H.; Salomon, E.; Kahn, A.; Cahen, D. *Adv. Mater.* **2008**, *20*, 3931–3936.
(32) Salomon, A.; Boecking, T.; Chan, C. K.; Amy, F.; Girshevitz, O.; Cahen, D.; Kahn, A. *Phys. Rev. Lett.* **2005**, *95*, 266807/266801–266807/266804.
(33) Coropceanu, V.; Cornil, J.; Filho, D. A. S.; Oliver, Y.; Silbey, R.; Bredas, J.-L. *Chem. Rev.* **2007**, *107*, 926–952.
(34) Li, G.; Shrotriya, V.; Huang, J.; Yao, Y.; Moriarty, T.; Emery, K.; Yang, Y. *Nat. Mater.* **2005**, *4*, 864–868.
(35) Peet, J.; Kim, J. Y.; Coates, N. E.; Ma, W. L.; Moses, D.; Heeger, A. J.; Bazan, G. C. *Nat. Mater.* **2007**, *6*, 497–500.
(36) Cho, J. H.; Lee, J.; Xia, Y.; Kim, B.; He, Y.; Renn, M. J.; Lodge, T. P.; Frisbie, C. D. *Nat. Mater.* **2008**, *7*, 900–906.
(37) Yan, H.; Chen, Z.; Zheng, Y.; Newman, C.; Quinn, J. R.; Dotz, F.; Kastler, M.; Facchetti, A. *Nature* **2009**, *457*, 679–686.
(38) Shen, Z.; Burrows, P. E.; Bulovic, V.; Forrest, S. R.; Thompson, M. E. *Science* **1997**, *276*, 2009–2011.
(39) Sirringhaus, H.; Tessler, N.; Friend, R. H. *Science* **1998**, *280*, 1741–1744.
(40) Tuccitto, N.; Ferri, V.; Cavazzini, M.; Quici, S.; Zhavnerko, G.; Licciardello, A.; Rampi, M. A. *Nat. Mater.* **2009**, *8*, 41–46.
(41) Lafferentz, L.; Ample, F.; Yu, H.; Hecht, S.; Joachim, C.; Grill, L. *Science* **2009**, *323*, 1193–1197.
(42) Davis, W. B.; Svec, W. A.; Ratner, M. A.; Wasielewski, M. R. *Nature* **1998**, *396*, 60–63.
(43) Nitzan, A. *Annu. Rev. Phys. Chem.* **2001**, *52*, 681–750.
(44) Bixon, M.; Jortner, J. *J. Chem. Phys.* **1997**, *107*, 5154–5170.
(45) Segal, D.; Nitzan, A.; Davis, W. B.; Wasielewski, M. R.; Ratner, M. A. *J. Phys. Chem. B* **2000**, *104*, 3817–3829.

architecture and the nature of the polaronic charge carriers. Overall, the current work demonstrates that the imine synthesis chemistry is a general approach to building long wires with different molecular subunits. This versatile chemistry, in combination with a simple and reproducible measurement method (CP-AFM), opens new opportunities to carefully examine the relationship between wire conductivity and molecular architecture in the hopping regime.

Experimental Section

Materials. Gold nuggets (99.999% pure) were purchased from Mowrey, Inc. (St. Paul, MN). Evaporation boats and chromium evaporation rods were purchased from R. D. Matthis (Long Beach, CA). Silicon (100) wafers were purchased from WaferNet (San Jose, CA). Contact mode AFM tips (DNP or NP silicon nitride probes) were purchased from Veeco Instruments (Camarillo, CA). Absolute ethanol was purchased from Fisher Scientific. Fluorene-2,7-diamine (FDA) was purchased from Aldrich, and naphthalene-2,6-dicarboxaldehyde (NDC) was synthesized as in the literature.[46] The compound was a light yellow solid and was recrystallized in acetone/H_2O with 72% overall yield.

Growth and Characterization of Molecular Wires. The Au substrates were 1000 Å thick films on silicon (with a 50 Å Cr adhesion layer) prepared in a Balzers thermal evaporator at a rate of 1.0 Å/s at a base pressure of $\leq 2 \times 10^{-6}$ Torr. The metal films were immersed for 18−24 h in 10 mL of 1 mM solutions of 4-aminothiophenol (ATP) in argon purged absolute ethanol. After removing the sample from the solutions and immersing with absolute ethanol for a half hour to get rid of physisorbed molecules, the sample was immersed in 10 mM of NDC solution in absolute ethanol for 24 h at 40 °C to ensure the complete formation of imine bonds. The sample was then immersed in absolute ethanol for 1 h, and the same procedure was followed in 10 mM of FDA solution in absolute ethanol. Wire molecular lengths were controlled with the number of the alternating additions of NDC and FDA on Au substrates. Odd and even ONI wires were end-capped with benzaldehyde and aniline, respectively. All ONI wires were rinsed with absolute ethanol and dried under a stream of N_2 before all measurements.

ONI wires were characterized by ellipsometry, X-ray photoelectron spectroscopy (XPS), reflection−absorption Fourier transform infrared spectroscopy (RAIRS), and cyclic voltammetry. Ellipsometry measurements were carried out on a VASE spectroscopic ellipsometer (J. A. Woollam Co., Inc.). Measurements of the polarization angles (Ψ and Δ) were taken as a function of wavelength (λ) between 600 and 1000 nm at an incident angle of 65°. The indices of refraction ($n(\lambda)$) and extinction coefficients ($k(\lambda)$) of the Au-coated substrates were determined by measurement of the polarization angles prior to monolayer deposition and wire growth. The instrument software converted these values to $n(\lambda)$ and $k(\lambda)$ of Au films and saved them as a material file. After monolayer formation and wire growth on Au substrates, the polarization angles were measured again and the film thicknesses were determined by a built-in algorithm. The $n(\lambda)$ and $k(\lambda)$ of the SAMs were assumed to be 1.45 and 0, respectively, over the 600−1000 nm wavelength range.

XPS spectra were taken on a Perkin-Elmer Phi 5400 spectrometer with a Mg Kα X-ray source (1253.6 eV) using a hemispherical analyzer in an ultrahigh vacuum ($<10^{-9}$ Torr) system. The X-ray anode was operated at 200 W, and the analyzer was set at a pass energy of 89.45 eV for survey scans and 17.9 eV for high-resolution scans. The binding energy scales were referenced to the $Au_{4f7/2}$ peak (84.0 eV). The monolayer thickness was calculated using the relative intensities of the Au_{4f} and C_{1s} peak and by using a hexadecanethiol SAM on Au as a reference ($d = 1.86$ nm). As we will discuss later, similar surface coverages ($\sim 4 \times 10^{-10}$ mol/cm^2)[47] of both SAMs allow us to use a hexadecanethiol SAM as a reference in the estimation of ONI monolayer thickness. Assuming the same attenuation length of gold ($\lambda_{Au} = 3.46$ nm) and carbon ($\lambda_C = 3.02$ nm) photoelectrons for the reference and wire monolayers, calculation based on eq 1 yielded the thickness.[48−50]

$$\frac{\frac{I_C}{I_{Au}}(\text{sample})}{\frac{I_C}{I_{Au}}(\text{reference})} = \frac{\left\{1 - \exp\left(-\frac{d_{\text{sample}}}{\lambda_C}\right)\right\} \exp\left(-\frac{d_{\text{reference}}}{\lambda_{Au}}\right)}{\exp\left(-\frac{d_{\text{sample}}}{\lambda_{Au}}\right)\left\{1 - \exp\frac{d_{\text{reference}}}{\lambda_C}\right\}} \quad (1)$$

where I_C = the intensity of C_{1s} peaks, I_{Au} = the intensity of Au_{4f} peaks, and d is the thickness. The estimated length and film thickness measured by ellipsometry and XPS for all ONI wires are shown in Figure 3.

RAIRS was taken with a Nicolet Series II Magna-IR System 750 FTIR with a Harrick Seagull accessory for grazing angle specular reflectance measurements. The infrared beam was incident at 84° with respect to the surface normal. A total of 2000 scans were collected at 1.0 cm^{-1} resolution. RAIRS was used for monitoring stepwise imination, as shown in Figure 2b. Cyclic voltammetry (CV) experiments were undertaken to determine the redox states of ONI wires and to measure surface coverage. In these experiments, a three-neck electrochemical cell was used. A clean O-ring (1.0 cm diameter) surrounding a hole in the bottom of the cell was placed between the cell and a monolayer-coated Au substrate, which acted as the working electrode. The cell was filled with 0.2 M tetrabutylammonium hexafluorophosphate (Bu_4NPF_6) in purified acetonitrile which was deoxygenated by three cycles of freeze−pump−thaw treatments. A Pt wire was used as the counter electrode and the cell was referenced to Ag wire. Prior to examining the monolayer oxidation potentials, the system was calibrated to the ferrocene oxidation potential. For each monolayer, the scan was recorded at a sweep rate of 300 mV/s and the CV curves were reproducible and stable to electrochemical cycling within the range of −1.0 to +1.5 V vs Ag wire. In addition, the surface coverage (Γ) was determined according to eq 2[23]

$$\Gamma = \frac{Q}{nFA} \quad (2)$$

where Q is the charge injected into the SAM, n is the number of electrons involved in the electron-transfer process (n is taken to be 1), F is the Faraday constant, and A is the surface area of the monolayer examined, that is, the area inside of the O-ring. Q was obtained by integrating the area under the forward sweep of the cyclic voltammogram using the first oxidation wave for each wire.

Determination of Molecular Energy Levels. The electronic structures of ONI wires were determined by UV/visible spectroscopy and UV photoelectron spectroscopy (UPS) experiments. UV/visible absorption spectra were taken of the molecular films on semitransparent thin Au films using a Beckman Coulter DU720 UV/visible spectrometer. Twenty nm thick Au films were thermally deposited on a polystyrene UV cell. Molecular films were formed on the Au film in the same way described above. Figure S1 shows the UV/visible absorption spectra for all ONI wires, and their optical gaps obtained from the absorption edge are given in Table 1.

UPS spectra were taken with He I ($h\nu = 21.2$ eV) radiation incident at 45° from the sample normal to examine the electronic

(46) Hagiya, K.; Mitsui, S.; Taguchi, H. *Synthesis* **2003**, *6*, 823.

(47) Bain, C. D.; Troughton, E. B.; Tao, Y.-T.; Evll, J.; Whitesides, G. M.; Nuzzo, R. G. *J. Am. Chem. Soc.* **1989**, *111*, 321–335.

(48) Laibinis, P. E.; Bain, C. D.; Whitesides, G. M. *J. Phys. Chem.* **2002**, *95*, 7017–7021.

(49) Bain, C. D.; Whitesides, G. M. *J. Phys. Chem.* **2002**, *93*, 1670–1673.

(50) Fuxen, C.; Azzam, W.; Arnold, R.; Witte, G.; Terfort, A.; Woll, C. *Langmuir* **2001**, *17*, 3689–3695.

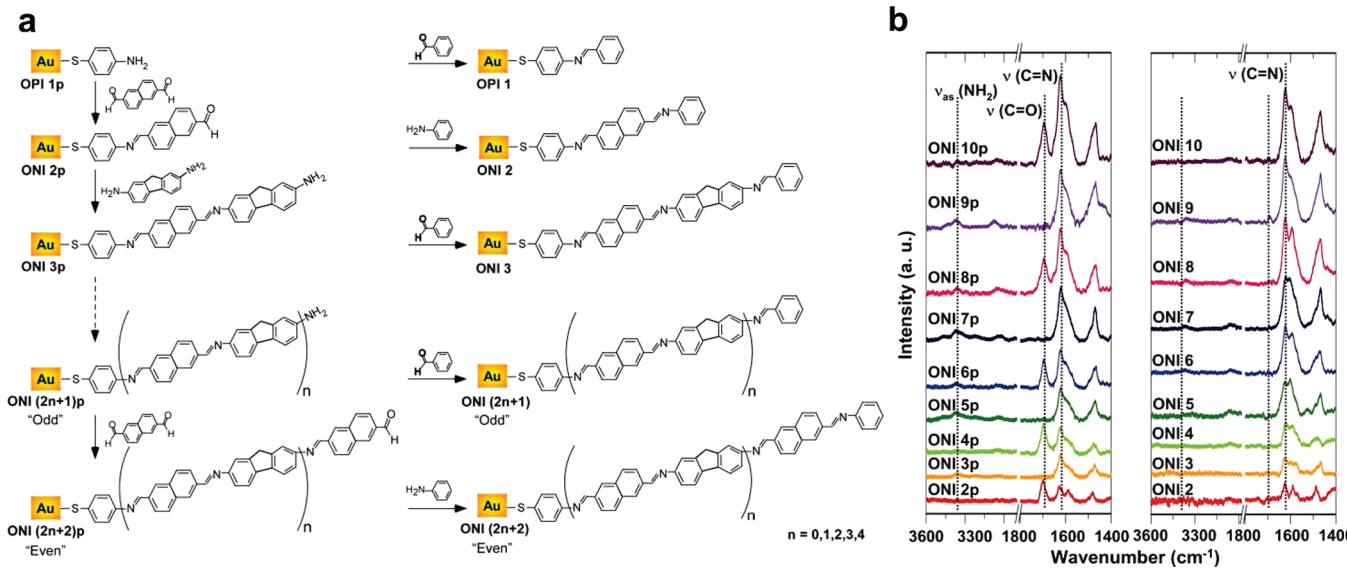

Figure 2. (a) Molecular structure and synthetic route to ONIp and ONI monolayers on Au substrates. (b) RAIRS spectra of ONIp (left) and ONI monolayers (right). Vertical dashed lines indicate positions of the symmetric amine stretch (NH_2, 3360 cm^{-1}), carbonyl stretch (C═O, 1697 cm^{-1}), and imine stretch (C═N, 1620 cm^{-1}). Peaks for NH_2 and C═O appear in the uncapped ONIp wires with odd and even numbers of repeat units, respectively.

Table 1. Redox Properties and Energy Level Alignments of ONI Wires[a]

monolayer	oxidation potentials (V)	AIP (eV)	surface coverage (× 10^{-10} mol/cm^2)	E_g (eV)	E_{vert} (eV)	$E_F - E_{HOMO}$ (eV)
ONI 2	0.22	7.23	3.1	3.0	3.74	0.5
ONI 3	0.06	6.78	3.6	2.6	3.50	0.5
CB ONI 3				3.2		0.7
ONI 4	–0.13	6.77	3.8	2.6	3.43	0.5
ONI 5	–0.15	6.74	4.2	2.5	3.38	0.4
ONI 6	–0.15	6.74	4.6	2.5	3.36	0.4
CB ONI 6				2.6		0.5
ONI 7	–0.17	6.70	4.9	2.4	3.34	0.4
CB ONI 7				2.6		0.5
ONI 8	–0.20	6.70	5.1	2.4	3.33	0.3
ONI 9	–0.22	6.67	5.0	2.4	3.32	0.3
ONI 10	–0.25	6.67	4.8	2.4	3.31	0.3

[a] The oxidation potentials were determined from lower edge of the oxidation peak of ONI wires referenced to ferrocenium/ferrocene (Fc^+/Fc). The energy offsets ($E_F - E_{HOMO}$) and optical gaps (E_g) are determined from onset of UPS and UV−vis spectra, respectively. Adiabatic ionization potential (AIP, eV) and first vertical transition (E_{vert}, eV) energies for the ONI wires as determined at the M062X/6-31G** level of theory are also provided.

structure of ONI wires. Photoemitted electrons were collected at normal emission with a pass energy of 4.45 eV. All spectra were acquired at an applied bias of −7 V on the sample and the energy scale was referenced to the Fermi level of Au (E_F). The intensities of the raw spectra were normalized at E_F.

Electrical Measurements. Molecular junctions were formed by bringing an Au-coated tip into contact with a wire SAM. These experiments were performed with a multimode AFM from Veeco Instruments in a glovebox (O_2 < 8 ppm). A 2 nN load force was used to make a soft contact. Au-coated tips were prepared as reported previously.[51] The room temperature $I-V$ characteristics were examined up to ±1.5 V for the entire set of ONI wires. The resistance was determined from the linear $I-V$ relationship within the range of ±0.1 V. Three Au-coated AFM tips having a radius of ∼50 nm were used for the measurements, each of which gave the same resistance value for tunneling through an octanethiol SAM (an effective calibration standard). The three tips were used separately to examine three sets of wires: ONI 1−3 (tip 1), ONI 3−7 (tip 2), and ONI 7−10 (tip 3). Note that ONI 3 and 7 were each measured with two different tips to confirm that the same resistances were obtained. The number of molecules in each junction was estimated from the size of the tip radius and the wire surface coverage to be ∼100.[52]

Variable temperature measurements of the ONI wire resistances were performed with an environmentally controlled Molecular Imaging PicoScan/PicoSPM. We have checked that the tunneling current of the octanethiol SAM remains constant within ±10%[25] from a set point temperature of −30 °C (243 K) to room temperature at <5% relative humidity. Two different sample stages, a normal heating stage and a peltier cooling stage, were used to vary the temperature above and below room temperature, respectively. Silver paste was painted at the edge of each sample to make thermal contact between the sample and stage. The measured temperatures on the samples were consistent with the set point temperatures. The resistances shown in Figure 7 were determined from linear $I-V$ relationships within the range of ±0.1 V, and are the average values of resistances obtained at six different locations on the samples. Two Au-coated AFM tips having a radius of ∼50 nm were used for the measurements, each of which gave the same resistance value for tunneling through an octanethiol SAM and ONI 3. The two tips were used separately to examine the resistances of ONI 3, 4, 5, 7, and 10 in two temperature ranges: 245−293 K (tip

(51) Engelkes, V. B.; Beebe, J. M.; Frisbie, C. D. *J. Phys. Chem. B* **2005**, *109*, 16801–16810.

(52) Beebe, J. M.; Engelkes, V. B.; Miller, L. L.; Frisbie, C. D. *J. Am. Chem. Soc.* **2002**, *124*, 11268–11269.

1) and 303−333 K (tip 2). Note that all measurements were performed while keeping the relative humidity of chamber below 5%.

Computational Methods. Analysis of the ground neutral and radical-cation states of the ONI oligomer structures were carried out using density functional theory (DFT); for comparison, the OPI oligomer structures were also examined. The B3LYP[53−55] and MO62X[56] functionals were used in conjunction with the 6-31G** basis set. Time-dependent DFT (TD-DFT) was used to determine the vertical energies, oscillator strengths, and electronic configurations of the first excited states. The geometric and electronic structure parameters determined with the two functionals (e.g., oligomer backbone twist, bond-length alternation changes on oxidation, adiabatic/vertical ionization potentials, molecular orbital densities and eigenvalues, and vertical transition energy to the first excited state) showed similar trends. Data derived with the M062X functional are reported herein, with all M062X and B3LYP data provided in the Supporting Information. Electronic density of states (DOS) for the oligomers were determined by convoluting the one-electron occupied molecular orbital eigenvalues with Gaussian functions characterized by a full width at half-maximum (fwhm) of 0.5 eV.[57−59] All calculations were performed with Gaussian 09 (revision A.02),[60] and molecular orbital density plots were generated with ArgusLab 4.0.1.[61]

Results and Discussion

Growth and Characterization of Molecular Wires. ONI wires were prepared from an Au substrate using the aryl imine chemistry with alternate addition of 2,6-naphthalenedicarboxaldehyde and 2,7-fluorenediamine, as shown in Figure 2a. Each ONIp wire terminated with $-NH_2$ or $-CHO$ groups was end-capped with benzaldehyde or aniline, respectively. The end-capping provided a consistent terminal group throughout the ONI series that facilitated reproducible electrical characterization.

The growth of wires was monitored using reflection−absorption Fourier transform infrared spectroscopy (RAIRS). The RAIRS data, shown in Figure 2b (left), reveal the alternate appearance and disappearance of carbonyl stretches (1697 cm^{-1}) and symmetric amine stretches (3360 cm^{-1}) in ONIp molecules, which verified the imination mechanism and indicated near quantitative reaction of all exposed reactive end groups. The intensity of imine stretching (1620 cm^{-1}) and the benzene ring vibrational mode (1470 cm^{-1}) increased with the number of repeat units, as expected. Complete end-capping was confirmed by the disappearance of the terminal group vibrational modes in Figure 2b (right).

In addition, ONI monolayers were extensively characterized by ellipsometry, X-ray photoelectron spectroscopy (XPS), and cyclic voltammetry (CV). Key results are shown in Figures 3 and 4 and compiled in Table 1. Importantly, monolayer

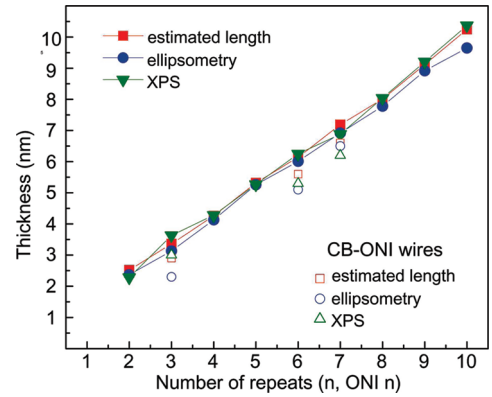

Figure 3. Measured thicknesses and estimated lengths for ONI wires and conjugation broken (CB) ONI wires. The structures of CB ONI wires are given in Figure 7. Blue circles and green inverse triangles indicate the measured thickness, respectively, by ellipsometry and XPS. The estimated lengths are represented in red squares and were obtained with the Cambridge Scientific Chem3D software. Molecular length is the terminal H to S distance plus the Au−S bond length. The Au−S bond length was taken to be 2.36 Å.[62]

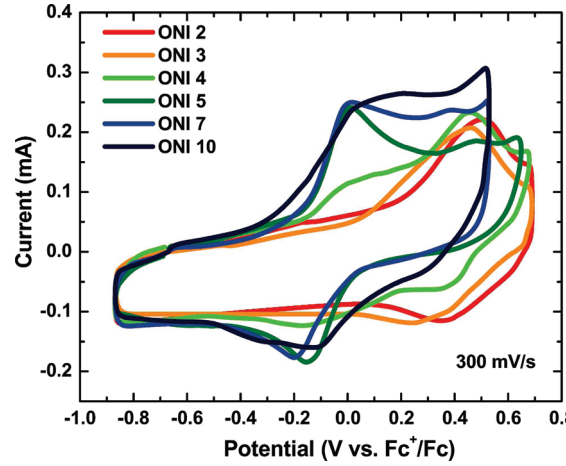

Figure 4. Cyclic voltammograms of selected ONI wires obtained in 0.2 M Bu_4NPF_6/CH_3CN. The reference and counter electrodes were Ag wire and Pt wire, respectively. The scan rate was 300 mV/s.

thicknesses from ellipsometry and XPS measurements have a very nice correlation with the estimated length (Figure 3), which indicates that the wires grow with an upright (essentially untilted) orientation with respect to the Au substrate. The molecular lengths determined from the M062X/6-31G** geometry optimization agree well with the empirically determined data (Table S8, Supporting Information).

The ONI wires are redox-active, as demonstrated by the cyclic voltammograms (CV) of selected wires in Figure 4. The potentials of the oxidation states and the estimated surface coverages for each ONI wire are tabulated in Table 1. All oxidation peaks were reversible within the range of −0.9−0.7 V versus ferrocenium/ferrocene (Fc^+/Fc), and no reduction was detected within the solvent electrochemical window for all ONI wires. The oxidation peak shifts to lower potential as wire length increases, which is largely expected based on the increased conjugation length. These results are confirmed by the adiabatic ionization potential energies determined at the M062X/6-31G**

(53) Becke, A. D. *J. Chem. Phys.* **1993**, *98*, 5648–5652.
(54) Becke, A. D. *Phys. Rev. A: At. Mol. Opt. Phys.* **1988**, *38*, 3098–3100.
(55) Lee, C.; Yang, W.; Parr, R. G. *Phys. Rev. B: Condens. Matter* **1987**, 785–789.
(56) Zhao, Y.; Truhlar, D. G. *Theor. Chem. Acc.* **2008**, *120*, 215–241.
(57) Risko, C.; Zangmeister, C. D.; Yao, Y.; Marks, T. J.; Tour, J. M.; Ratner, M. A.; van Zee, R. D. *J. Phys. Chem. C* **2008**, *112*, 13215–13225.
(58) Zhan, X.; Risko, C.; Amy, F.; Chan, C.; Zhao, W.; Barlow, S.; Kahn, A.; Bredas, J.-L.; Marder, S. R. *J. Am. Chem. Soc.* **2005**, *127*, 9021–9029.
(59) Chan, C. K.; Kim, E.-G.; Bredas, J.-L.; Kahn, A. *Adv. Funct. Mater.* **2006**, *16*, 831–837.
(60) Frisch, M. J.; et al. *Gaussian 09*, revision A.02; Gaussian, Inc.: Wallingford, CT, 2009.
(61) Thompson, M. A. *ArgusLab 4.0.1*, Planaria Software LLC: Seattle, WA.
(62) Tour, J. M.; Jones, L.; Pearson, D. L.; Lamba, J. J. S.; Burgin, T. P.; Whitesides, G. M.; Allara, D. L.; Parikh, A. N.; Atre, S. *J. Am. Chem. Soc.* **1995**, *117*, 9529–9534.

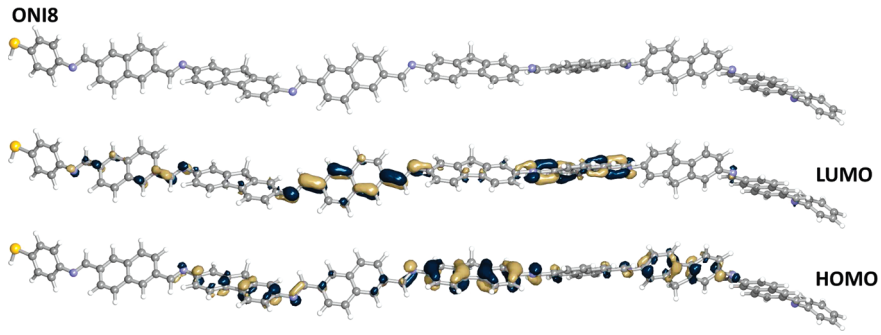

Figure 5. Pictorial representation of the ground-state geometry (top) and HOMO and LUMO molecular orbital densities (bottom) for ONI 8 as determined at the M062X/6-31G** level of theory.

level of theory (see Table 1). Integration of the CV sweeps of the ONI wires reveals nearly identical surface coverage (3.1×10^{-10} to 5.1×10^{-10} mol/cm^2) over the entire set of wires. These surface coverage data indicate that the number of molecular wires contacted by the electrodes in junction experiments varies by a factor of 2 or so, and thus differences in the magnitude of measured current cannot be explained by surface coverage arguments in the analysis of CP-AFM data. Collectively, the surface characterization data indicate that quality monolayers of ONI wires were prepared.

Energy Level Alignment. The electronic structures of ONI wires were examined with ultraviolet−visible (UV−vis) absorption spectroscopy and ultraviolet photoelectron spectroscopy (UPS). Oligo or poly(arylazomethine) molecules generally exhibit a twisted conformation mostly due to the steric interaction between hydrogen atoms on adjacent aromatic rings. Previously, we reported based on UV−vis absorption data that electronic delocalization extends only over three repeating units of OPI wires, presumably because of their nonplanar conformation.[23] For ONI wires, the optical band gap (E_g) is significantly reduced with molecular length up to ONI 3, which indicates that electronic coupling between adjacent fluorene and naphthalene building blocks is very strong (Table 1).

The optical gaps for wires longer than ONI 3 are more gradually reduced up to ONI 7, and remain constant at 2.4 eV for ONI 8−10 (Table 1); similar trends are shown with the TD-DFT calculations, with the electronic configuration of the first excited state being predominantly a HOMO→LUMO transition. Collectively, these results indicate that there is significant π-orbital coupling along the ONI chains, but that shorter segments may be more strongly coupled, as could be expected. We note that the optical band gaps in ONI wires are relatively smaller by 0.1−0.2 eV compared to those in the analogous OPI wires;[23] the vertical transition energies from the TD-DFT calculations of both the ONI and OPI wires reveal a similar result. This bathochromic shift has been observed in various oligoimine systems when phenylene rings are replaced by naphthalenes or fluorenes.[63−65] The electronic coupling in ONI wires is enhanced by the contribution of highly conjugated building blocks, which is consistent with lower oxidation potentials in the CV measurements.

The energy offsets ($E_F - E_{HOMO}$) between the Au Fermi level (E_F) and the highest occupied molecular orbital (HOMO) (E_{HOMO}) were determined over the entire set of ONI wires (Table 1). As the wires become longer, $E_F - E_{HOMO}$ is reduced from 0.5 to 0.3 eV, which is also consistent with the observed trend in oxidation potentials. The barrier heights at the interface of ONI wires are smaller compared to an interfacial barrier energy of 0.7 eV in OPI wires.[23] While the smaller barrier may result in higher ONI wire conductivity, as discussed below, it is important to recognize that barriers in the metal−molecule−metal junctions may be even lower than the barrier determined for the single metal−wire interface.[4,5,66] That is, additional metal−molecule charge transfer can occur when making the second contact, and naturally this is not accounted for in UPS measurements of molecule−metal interfaces.

Conformation of the Wires. Quantum chemical calculations on isolated ground-state configurations of the ONI wires reveal their highly twisted structure, Figure 5. Torsion angles about the C−N bonds in the wires are typically 38−40° (see Table S1 in Supporting Information), which indicate that, in spite of substantial steric interactions, π-electronic coupling between the naphthalene and fluorene building blocks remains significant.[67] Of course, the calculations only take into account a static, isolated picture of the oligomeric structures and do not account for the dynamic processes within the junction. The conformations of the wires in the junction will most certainly be affected by intermolecular interactions and the pressure applied by the CP-AFM tip (∼100 MPa).

Length Dependent Resistances. We investigated the transport characteristics of ONI wires using CP-AFM as shown in the inset to Figure 6a; CP-AFM has been used previously to measure conduction in a variety of molecular systems including OPI wires.[23−25,51,68,69] A current−voltage ($I-V$) sweep generally yielded a sigmoidally shaped curve as will be shown later, but over a small voltage range (±0.1 V) the $I-V$ response was linear. The resistances shown in Figure 6 are low voltage resistances determined over this small range, and averaged for 20 $I-V$ traces. In the linear plot of resistance (R) versus molecular length (L) (Figure 6a), a clear transition in the length dependence of resistances is exhibited near 4 nm (ONI 4), implying a change of transport mechanism. For long wires (ONI 4−ONI 10), the linear relationship of the resistance as a function of length suggests that hopping transport prevails in this

(63) Liu, C.-L.; Chen, W.-C. *Macromol. Chem. Phys.* **2005**, *206*, 2212–2222.
(64) Andres, S.; Guarin, P.; Dufresne, S.; Tsang, D.; Sylla, A.; Skene, W. G. *J. Mater. Chem.* **2007**, *17*, 2801–2811.
(65) Schulze, J.; Gerson, F.; Murrell, J. N.; Heilbronner, E. *Helv. Chimi. ACTA* **1961**, *44*, 428–441.
(66) Kaasbjerg, K.; Flensberg, K. *Nano Lett.* **2008**, *8*, 3809–3814.
(67) Bredas, J.-L.; Street, G. B.; Themans, B.; Andre, J. M. *J. Chem. Phys.* **1985**, *83*, 1323–1329.
(68) Leatherman, G.; Durantini, E. N.; Gust, D.; Moore, T. A.; Moore, A. L.; Stone, S.; Zhou, Z.; Rez, P.; Liu, Y. Z.; Lindsay, S. M. *J. Phys. Chem. B* **1999**, *103*, 4006–4010.
(69) T, W.; Kelley; Granstrom, E.; Frisbie, C. D. *Adv. Mater.* **1999**, *11*, 261–264.

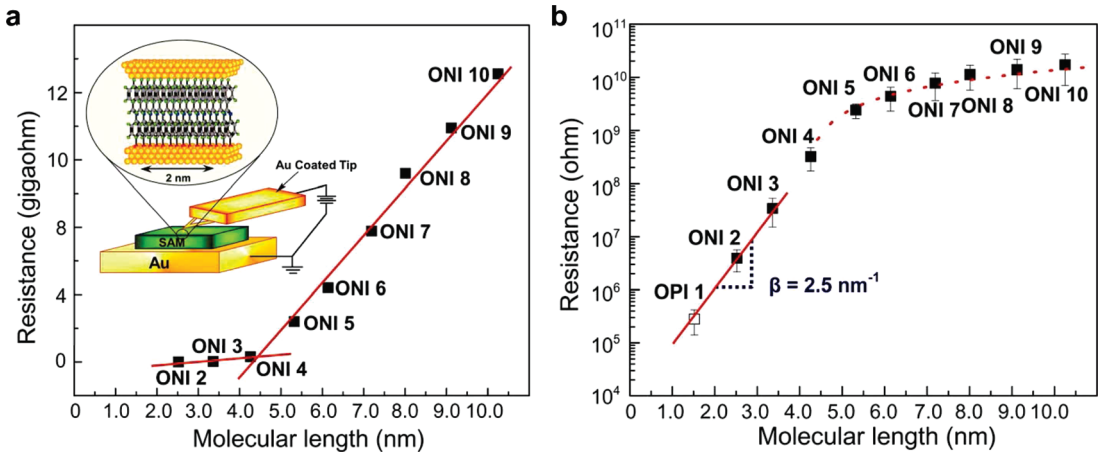

Figure 6. Measurements of molecular wire resistance by conducting probe atomic force microscopy (CP-AFM). (a) A plot of R versus L for the Au/wire/Au junctions. Each data point is the average differential resistance obtained from 20 $I-V$ traces in the range −0.1 to +0.1 V. Straight lines are linear fits to the data. Inset: An Au-coated tip was brought into contact with an ONI monolayer on Au. $I-V$ traces were obtained over ±1.5 V at a load of 2 nN on the tip contact. (b) Semilog plot of R versus L for the Au/wire/Au junctions. Each data point is the average differential resistance obtained from 20 $I-V$ traces in the range −0.1 to +0.1 V. Error bars represent one standard deviation. The straight line is a linear fit to the data according to eq 2. The dashed line indicates a linear fit obtained in (a) for long ONI wires.

regime.[43,45] This linear dependence is indicated by the dashed line in the semilog plot of R versus L (Figure 6b). Figure 6b reveals that the resistances for long wires have much weaker length dependence than those for short molecules, as expected for hopping transport. From the slope of R versus L in Figure 6a and the estimated number of wires in the junction (∼100),[52] we calculated a single-wire conductivity of $(1.8 \pm 0.1) \times 10^{-4}$ S/cm.

It is important to note that this value may be influenced by intermolecular interactions. Recently, Landau et al. used a computational approach to investigate the role of intermolecular interactions on molecular conduction.[70] They had two main findings. First they determined that the conductance per molecule in an adlayer can differ substantially from the conductance of a single, isolated molecule. However, the single molecule conductance can be either greater or less than the conductance per molecule in an adlayer depending on the details of the metal-molecule coupling (broadening of energy states) and the Fermi level alignment in the junction. Second, they found that conductances of parallel molecular wires can be summed (so-called linear scaling) provided that the junction incorporates at least a few tens of molecules. Our calculation of single-wire conductivity thus has to be interpreted in this context, namely that the measurement involved many molecules (∼100), and measurements on isolated ONI wires may yield different estimates of the wire conductivity. Nevertheless, within the uncertainty of our measurement, the conductivity of ONI wires is higher than that of OPI wires ($(1.0 \pm 0.1) \times 10^{-4}$ S/cm),[23] suggesting that ONI wires are more efficient hopping conductors than OPI wires.

For short molecules (ONI 2, ONI 3), the semilog plot of R versus L in Figure 6b clearly displays that the resistances increase exponentially with length, as expected for a nonresonant tunneling process. In this case, R is well described by

$$R = R_0 \exp(\beta L) \qquad (2a)$$

where R is the junction resistance, R_0 is the effective contact resistance, L is molecular length, and β is the tunneling attenuation factor that depends on the nature of bonding in the molecular backbone.[24,25,52,71,72] The β value obtained from a linear fit is 2.5 nm^{-1}, smaller than the value obtained for short OPI molecules, 3.0 nm^{-1},[23] and indicates that tunneling through ONI molecules is more efficient than OPI molecules. This is consistent with the lower energy offset ($E_F - E_{HOMO}$) of short ONI molecules relative to short OPI molecules, which should reduce the effective tunneling barrier height.

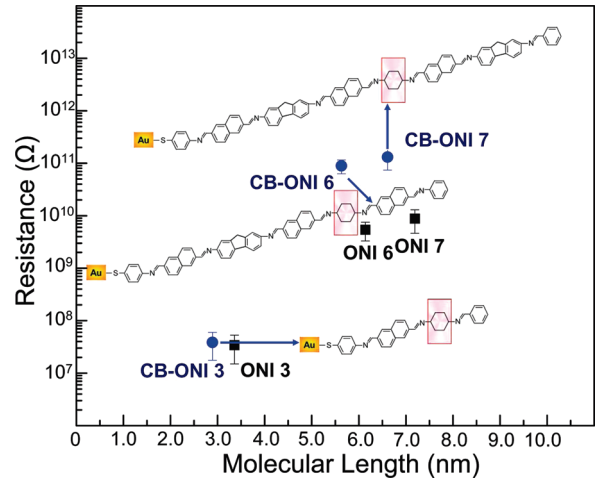

Figure 7. A semilog plot of R versus L for Au/ONI/Au junctions and conjugation broken Au/CB ONI/Au junctions. Each data point is the average differential resistance from 20 $I-V$ traces in the interval −0.1 to +0.1 V. Error bars represent one standard deviation. The blue circles are the resistances of conjugation-broken ONI (CB ONI) wires. Pink boxes indicate the position where conjugation is broken.

Conjugation Broken ONI Wires (CB ONIs). For the purpose of examining the sensitivity of conduction to wire architecture, we prepared a set of engineered wires that incorporate a deliberate conjugation breaking (CB) link (an aliphatic cyclohexyl group) within the ONI backbone (CB ONIs). The structure of CB ONI wires and their low-voltage resistances are shown in Figure 7. The conduction in the long wires is much more

(70) Landau, A.; Kronik, L.; Nitzan, A. *J. Comput. Theor. Nanosci.* **2008**, *5*, 535–544.

(71) Wold, D. J.; Haag, R.; Rampi, M. A.; Frisbie, C. D. *J. Phys. Chem. B* **2002**, *106*, 2813–2816.

(72) Wold, D. J.; Frisbie, C. D. *J. Am. Chem. Soc.* **2001**, *123*, 5549–5556.

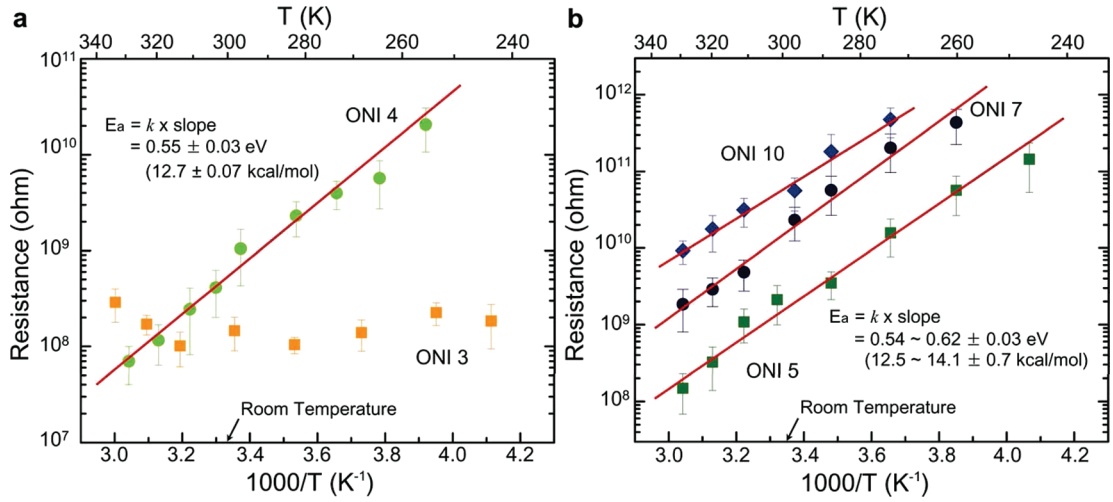

Figure 8. Arrhenius plot for (a) ONI 3 and ONI 4 and (b) ONI 5, ONI 7, and ONI 10. Each data point is the average differential resistance obtained at six different locations of samples in the range −0.1 to +0.1 V. Error bars represent one standard deviation. Straight lines are linear fits to the data.

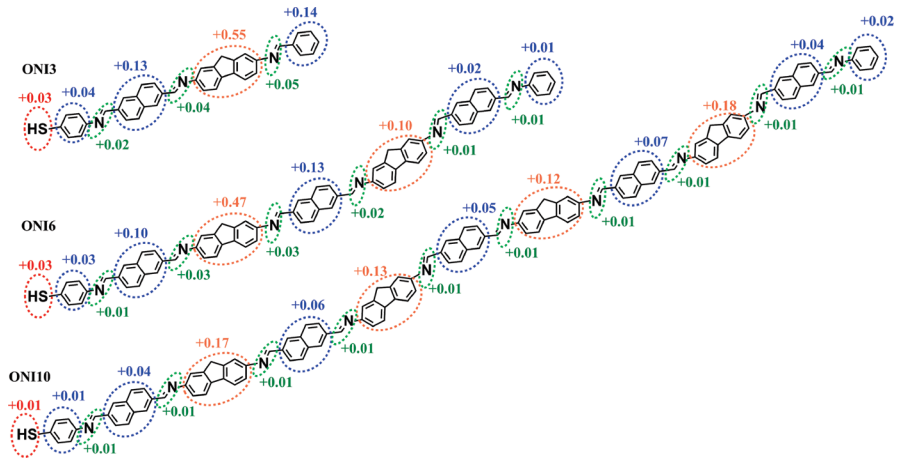

Figure 9. Pictorial representation of excess positive charge distributions for selected ONI wires as calculated using the M062X/6-31G** level of theory. Charge values correspond to the differences in Mulliken atomic charges of the radical-cation state with respect to the neutral ground state.

sensitive to the presence of the cyclohexyl group than in the short molecules, as we previously demonstrated with an analogous OPI set (CB OPIs).[23] For CB ONI 3, the resistance is slightly increased compared to ONI 3, as expected, because the aliphatic cyclohexyl links raise the average tunneling barrier. In contrast, for the longer CB ONI 6 and CB ONI 7, the resistance change from the corresponding ONI 6 and ONI 7 wires is considerably greater, approximately 15 times greater. For hopping transport in the long wires, a large change in resistance is expected upon interrupting the conjugation because injected carriers now feel the energetic details of atomic orbitals though molecular backbone instead of averaging them, and the mismatched HOMO energy of the cyclohexyl group represents a significant hopping barrier. Overall, the conjugation blocking experiments confirm that conduction depends upon the bond architecture and they also support the conclusion that tunneling occurs in the short wires and hopping transport prevails in the long wires.

Temperature Dependent Resistance. Although a change in transport mechanism is apparent in the R versus L plot, the temperature dependence is key to verifying different transport mechanisms. Figure 8 shows an Arrhenius plot of R versus the inverse of temperature (T) for selected ONI wires. Clearly, the resistance for ONI 3 is independent of temperature from 246 to 333 K, as expected for tunneling. However, ONI 4 and longer wires (ONI 5, 7, and 10) display strongly thermally activated transport characteristic of hopping. The activation energies determined from the slopes of the data are nearly identical to each other at 0.54 to 0.62 ± 0.03 eV (12.5 to 14.1 ± 0.7 kcal/mol), which implies that the same rate-determining step for hopping transport is active in all of the wires regardless of the molecular lengths. Collectively, the data in Figures 6−8 provide unambiguous evidence for a change in transport mechanism from tunneling to hopping near 4 nm in ONI wire length. The temperature dependence and change in mechanism near 4 nm are similar to what we have observed previously with OPI wires.[23]

In an effort to understand the nature of the charge carriers and the hopping conduction process, we performed quantum chemical calculations on isolated, static, positively ionized ONI wires as a function of length (Figure 9). We found that positive charge is localized predominantly on the fluorene substituents in the backbone, which is consistent with the HOMO wave function shown in Figure 5. The molecule also remains relatively twisted in the ionized state (see Table S1 for torsional angles).

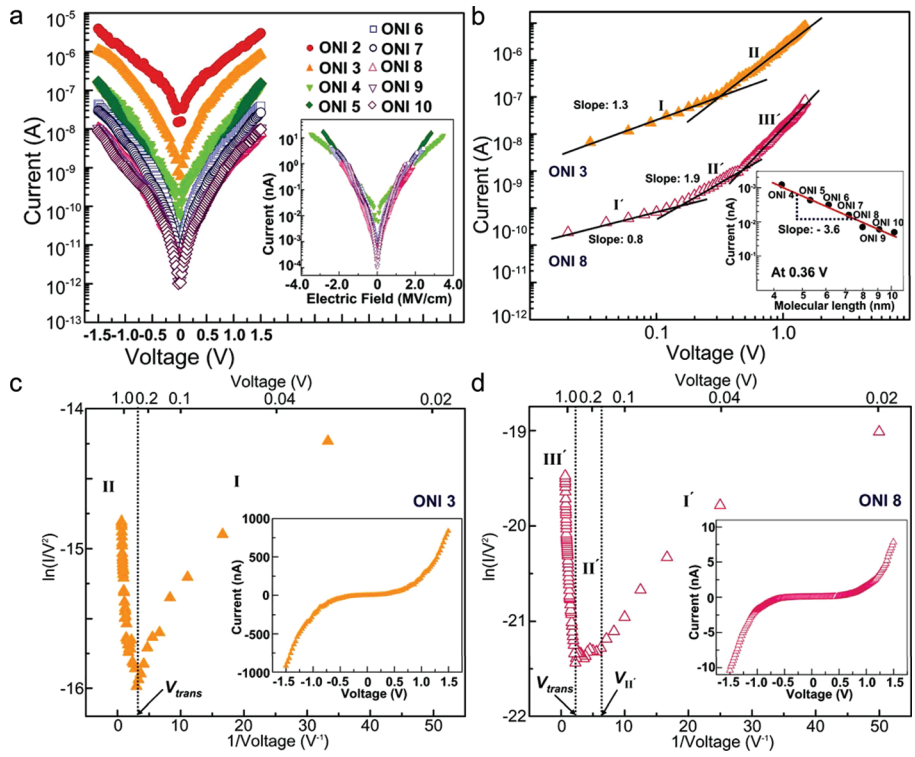

Figure 10. (a) Semilog plot of the average current for 20 $I-V$ traces for Au/ONI/Au junctions. The inset is a semilog plot of I versus electric field (E) for long ONI wires. (b) log−log plot of the average of 20 $I-V$ traces for the Au/ONI 3/Au and Au/ONI 8/Au junctions. Fits are shown in the different transport regimes. Inset: A log−log plot of I versus L obtained at 0.36 V for all long ONI wires, displaying the linear fit with a slope of −3.6 (0.36 V is the bias at which all long ONI wires are within regime II′). (c) Fowler−Nordheim plot for the ONI 3 data in (b). Two distinct regimes (I and II) are clearly observable with an inflection point at V_{trans}, indicating the switch from tunneling to field emission. The inset displays the sigmoidal $I-V$ curve on a linear scale. (d) Fowler−Nordheim plot for the ONI 8 data in (b). Three distinct regimes (I′, II′, and III′) are evident. The inset shows the sigmoidal $I-V$ curve.

According to the Marcus theory of electron transfer, the charge hopping rate (k_{et}) depends on the thermodynamic driving force ($\Delta G°$), which to a first approximation can be considered to correspond to the variations in hopping site energies, and the (polaronic) reorganization energy λ, as follows:

$$k_{et} \propto \exp\left(-\frac{(\lambda + \Delta G°)^2}{4\lambda k_B T}\right) \quad (3)$$

where k_B is the Boltzmann constant and T is the temperature. We have computed the relaxation energies λ_1 and λ_2 associated with adiabatic ionization and neutralization of the ONI wires, Table S2. Their sum, λ_t, provides an estimate of the intramolecular reorganization energy.[33] In addition, in a polarizable medium like a molecular junction in which there are of order 100 molecules in parallel, there will be an environmental (electronic and nuclear) polarization that contributes to λ in eq 3. In π-conjugated materials, this contribution is commonly estimated to have a magnitude similar to the intramolecular λ_t.[33]

If we consider the hopping sites in long ONI wires to be short conjugated subunits, we can make a rough estimate of the total λ. Taking λ_1 and λ_2 from the ONI 3 wires (we estimate the hopping sites to be ~3 units long because by UV−vis the decrease in the optical gap becomes more gradual beyond 3 units), we find λ_t to be 0.45 eV (see Table S4). Then if we double this value in order to account approximately for environmental contributions, we obtain $\lambda_{total} \sim 0.90$ eV. According to eq 3, we would predict that the total activation energy (E_a) is $(\lambda_{total} + \Delta G°)^2/4\lambda_{total}$. $\Delta G°$ can be estimated to be on the order of −25 meV, taking into account the effects of the applied electric field (at 0.1 V) across the junction. We thus obtain $E_a \sim 0.2$ eV, which is a factor of 2−3 lower than the measured activation energy.

It is generally known, however, that nuclear motions can be significantly hindered in the solid state relative to the liquid or gas phase, and this in turn can impact reorganization energies.[73,74] For example, the torsional barrier for $-CF_3$ rotation in 3-(trifluoromethyl)phenanthrene increases from 0.4 kcal/mol (17 meV) in the gas phase to 2.6 kcal/mol (112 meV) in the crystalline state, or a factor of 6.5. In this context, it is reasonable to suppose that molecular relaxation energies of the ONI wire molecules in a SAM sandwiched between metal contacts may be substantially greater than we have calculated here for isolated molecules. Clearly, more work will need to be done to determine the true nature of the hopping process in ONI wires, and in particular the origin of the activation energy. However, these estimations indicate that the magnitude of the measured activation energy is not unreasonable and it is indeed in approximate agreement with expectations based on molecular reorganization upon charge transfer.

Electric Field Dependent $I-V$ Characteristics. We have also carefully examined the voltage and electric field dependence of the $I-V$ characteristics of ONI wires (Figure 10). The semilog plot of I versus V in Figure 10a demonstrates that for short ONI molecules (ONI 2 and 3), there are larger decreases in current with wire length, whereas these changes become much smaller for the long wires (ONI 4−10). A plot of log I versus electric field (E) (see inset) reveals that the traces for the long wires collapse nearly on top of one another. This result indicates that for the long wires transport is field driven, as expected for a

Table 2. Analyses of *I*−*V* Characteristics for ONI Wires

monolayer	*n* in I and I′ $I \propto V^n$	*n* in II′ $I \propto V^n$	V_{trans} (V) [E_{trans} (MV/cm)]	$V_{II'}$ (V) [$E_{II'}$ (MV/cm)]	ϕ_{FE} (eV)
ONI 2	1.0		0.63 [2.5]		0.3− 0.5
ONI 3	1.3		0.33 [1.0]		0.3− 0.5
CB ONI 3	1.0		0.54 [1.9]		
ONI 4	0.9	2.7	0.90 [2.1]	0.28 [0.65]	0.2− 0.4
ONI 5	1.1	2.8	0.64 [1.2]	0.22 [0.42]	0.2− 0.4
ONI 6	1.2	2.3	0.54 [0.89]	0.14 [0.23]	0.2− 0.4
CB ONI 6	1.1	2.2	0.54 [0.96]	0.14 [0.25]	
ONI 7	1.0	2.3	0.48 [0.67]	0.14 [0.19]	0.1− 0.3
CB ONI 7	1.1	1.9	0.44 [0.67]	0.12 [0.18]	
ONI 8	0.8	1.9	0.44 [0.55]	0.12 [0.15]	0.1− 0.3
ONI 9	1.0	2.0	0.42 [0.46]	0.10 [0.11]	0.1− 0.3
ONI 10	1.0	2.0	0.42 [0.41]	0.10 [0.10]	0.1− 0.3

hopping mechanism in which the electric field pushes the carriers. In short molecules, voltage is the key parameter for the tunneling process.

As we demonstrated for OPI wires,[23] short and long ONI wires also exhibit different transport regimes in log−log plots of the *I*−*V* characteristics, Figure 10b. The data for ONI 3 reveal a transition at 0.33 V from linear (regime I) to nonlinear *I*−*V* behavior (regime II). In approximate terms, this transition arises from changes in the tunneling barrier shape from trapezoidal to triangular.[75,76] At low bias, the simple linear tunneling behavior is described by eq 4

$$I \propto V \exp\left(-\frac{2d\sqrt{2m_e\phi}}{\hbar}\right) \tag{4}$$

where d is the barrier width (wire length), m_e is the electron effective mass, and ϕ is the effective barrier height. Above the transition voltage $V_{trans} = 0.33$ V (regime II), the *I*−*V* behavior adapts to the Fowler-Nordheim (field emission) relation:

$$\ln\left(\frac{I}{V^2}\right) \propto \frac{-4d\sqrt{2m_e\phi^3}}{3\hbar q}\left(\frac{1}{V}\right) \tag{5}$$

where q is the elementary charge.

The change in mechanism to field emission for ONI 3 is clearly evident in the corresponding Fowler−Nordheim plot in Figure 10c. For low voltages (regime I), the current scales logarithmically with $1/V$ as predicted from eq 4, indicative of direct tunneling. Above V_{trans} (regime II), the current scales linearly with $1/V$ with a negative slope characteristic of field emission (eq 5). The transition point, V_{trans} (0.33 V) provides an estimate of the effective tunneling barrier height at $V = 0$. A compilation of V_{trans} values for different wires is included in Table 2. The V_{trans} values are smaller than those of the corresponding short OPI molecules (0.75 V in case of OPI 3)[23] and they also decrease with length, consistent with the trend in oxidation potentials and $E_F - E_{HOMO}$ offsets (see Table 1).

The longer ONI 8 wires exhibit three distinct transport regimes in Figure 10, panels b and d. The principal mechanisms governing these regimes were already proposed with long OPI wires.[23] Regimes I′ and III′ correspond to ohmic (field-driven) conduction and field emission, respectively, while regime II′ may correspond to space charge limited conduction (SCLC). In regime I′, the current scales linearly with voltage, characteristic of ohmic hopping conduction and consistent with the length and temperature dependent transport (Figures 6 and 8). The correspondence of regime III′ with field emission is evident in the Fowler−Nordheim plot in Figure 10d, where it is clear that at voltages above 0.6 V the plot has the expected negative slope. From the slope in regime III′, we calculated the emission barrier height (ϕ_{FE})[77] to be in the range of 0.1−0.3 eV assuming carrier effective mass ratios in the range 0.1 to 1.0, which are typical for molecular junctions.[14] This barrier is very much in line with measurements for the HOMO-to-Fermi level offset for long wires. Recall that $E_F - E_{HOMO}$ was determined to be 0.3−0.5 eV by UPS for long wires, but the expectation is that the real barrier for a junction will be lower.[78] The estimated emission barrier heights for the other long ONI wires are also listed in Table 2.

We propose that SCLC is responsible for regime II′, based on the slope of 1.9 in the log *I* versus log *V* plot (Figure 8b) and the slope of −3.6 in the log *I* versus log *L* plot at 0.36 V (inset in Figure 10b). Under bias, the carrier concentrations in the wires can be increased beyond their values in equilibrium. In SCLC transport, current scales with voltage and length as $I \propto V^2/L^3$, close to what we have observed in regime II′ (Table 2 and inset in Figure 10b). More detailed work will have to be done, however, to confirm the interpretation that SCLC transport is operative in regime II′.

Conclusion

We have measured DC electrical conduction in a set of conjugated oligoimine wires having systematically controlled lengths varying between 2.5 and 10.3 nm. These ONI wires exhibit electrical characteristics that are similar to previously reported OPI wires. In particular, there is a clear transition from tunneling to hopping transport near 4 nm in wire length, as evidenced by the length, temperature, and electric field dependence of the *I*−*V* characteristics. The wire resistance has an activation energy of 0.54−0.62 eV, which is two to three times higher than quantum chemical estimations of the reorganization energy associated with charge transfer among conjugated subunits in single, isolated chains. Because the conductance measurements involve ∼100 wire molecules, and not single

(73) Selzer, Y.; Cai, L.; Cabassi, M. A.; Yao, Y.; Tour, J. M.; Mayer, T. S.; Allara, D. L. *Nano Lett.* **2005**, *5*, 61–65.
(74) Wang, X.; Mallory, F. B.; Mallory, C. W.; Beckmann, P. A.; Rheingold, A. L.; Francl, M. M. *J. Phys. Chem. A* **2006**, *110*, 3954–3960.
(75) Beebe, J. M.; Kim, B.-S.; Gadzuk, J. W.; Frisbie, C. D.; Kushmerick, J. G. *Phys. Rev. Lett.* **2006**, *97*, 026801.
(76) Beebe, J. M.; Kim, B.-S.; Frisbie, C. D.; Kushmerick, J. G. *ACS Nano* **2008**, *2*, 827–832.
(77) Sze, S. M. *Physics of semiconductor devices*, 2nd ed.; John Wiley & Sons, Inc.: New York, 1981; Chapter 7.
(78) Rideout, V. L. *Thin Solid Films* **1978**, *48*, 261–291.

wires, intermolecular interactions may play a role in conduction. Overall, these experiments confirm that the oligoimine synthesis chemistry can be used to build wires that are long enough to probe the hopping regime and they open up significant opportunities to explore the connection between molecular structure and hopping transport in long wire architectures. Current efforts are aimed at understanding the roles of inter- and intramolecular steric interactions, electronic structures, and redox properties on hopping conduction.

Acknowledgment. The authors thank Greg Haugstad for support in the temperature dependent measurements, Prof. Xiaoyang Zhu for help with photoelectron spectroscopy, and Dr. Veaceslav Coropceanu for fruitful discussion. This work was supported primarily by the National Science Foundation under CHE-0616427. Partial support for facilities was provided by the NSF MRSEC program under Award Number DMR-0819885. Parts of this work were carried out in the Institute of Technology Characterization Facility, University of Minnesota, which receives partial support from NSF through the NNIN program.

Supporting Information Available: UV/visible and UPS spectra for all ONI wires and Tables for M062X/6-31G** and B3LYP/6-31G** data of ONI and OPI wires. This material is available free of charge via the Internet at http://pubs.acs.org.

JA910547C